Channel and Propagation Measurements at 300 GHz

Sebastian Priebe, Christian Jastrow, Martin Jacob, *Student Member, IEEE*, Thomas Kleine-Ostmann, Thorsten Schrader, *Member, IEEE*, and Thomas Kürner, *Senior Member, IEEE*

***Abstract*—Ultrabroadband Terahertz communication systems are expected to help satisfy the ever-growing need for unoccupied bandwidth. Here, we present ultra broadband channel measurements at 300 GHz for two distinct indoor scenarios, a point-to-point link of devices on a desktop and the connection of a laptop to an access point in the middle of an office room. In the first setup, measurements are taken with regard to distance, different antenna types and device displacements. Additionally, an interference constellation according to the two-ray model is examined. In the second setup, the focus is on the detection and characterization of the LOS- and the NLOS-paths in an indoor environment, including a maximum of two reflections. Temporal channel characteristics are examined with regard to maximum achievable symbol rates. Furthermore, ray obstruction due to objects in the transmission path is investigated.**

***Index Terms*—Channel modeling, channel sounding, diffraction, submillimeter channel measurements, THz communications, THz propagation measurements, THz system.**

I. Introduction

In the past years it has become obvious that wireless data rates exceeding 10 Gbit/s will be required in several years from now [1]. The opening up of carrier frequencies in the Terahertz range has been identified as most promising to provide sufficient bandwidths required for ultra fast and ultra broadband data transmissions [2], leading to the initiation of the IEEE 802.15 THz Interest Group (IG THz). A suitable frequency window can be found around 300 GHz, offering a currently unregulated bandwidth of 47 GHz [2]. As technological advance keeps up with the ever increasing demand for wireless data transmission capacity, electrical components for the generation of THz frequencies are already commercially available [3]. Based on subharmonic Schottky diode mixers, a 300 GHz transmission system has been set up at the Physikalisch-Technische Bundesanstalt, Braunschweig [4]. Experiments within the Terahertz Communications Lab (TCL) have proved the feasibility of an analog video transmission over 22 m [4] and a digital video data transmission over 52 m with a data rate of 96 Mbit/s [5]. A different approach to THz communication applying optical generation and modulation of frequencies between 300 and 400 GHz is reported in [6].

Primarily, three different scenarios can be identified for data communication at 300 GHz. The first one involves short distances up to 1 m as required for the wireless interconnection of different devices on a desktop or for ultrafast kiosk downloads. The second use case refers to THz indoor pico cells for wireless access as, e.g., imaginable in conference-, office-, or living rooms, whereas the third scenario is the wireless extension of wired backbone networks over ranges greater than 10 m [7]. Private applications will include high speed wireless data exchange with flash drives, the almost instant download of large files (e.g., HD films) and uncompressed video streaming of future ultra high resolution video formats [8]. Professional applications cover, e.g., fast file exchange on conferences, telemedicine, and the provision of interference-free wireless high speed networks in trade fair halls by dividing the huge available bandwidth into multiple subbands. THz waves can also be utilized for a wide range of different other applications apart from data transmission like, e.g., remote sensing, radio astronomy or security. A good overview can be found in [9].

Future THz WLANs will primarily rely on line-of-sight (LOS) conditions and high gain antennas with gains beyond 25 dBi to overcome the high free-space [10] and additional high reflection losses [11]. Sophisticated antenna designs are required to provide both high gain and the ability to serve multiple users at different positions. Here, a very promising approach are multibeam antennas (e.g., dielectric rod or ring-slot antennas) as shown in [12]. In case of LOS paths blocked by persons or objects, the concept of directed nonline-of-sight (NLOS) communication has been proposed [2]. Hence, not only LOS, but also NLOS channels will have to be characterized.

Employing bandwidths from several GHz up to several 10 GHz, channels at 300 GHz cannot be described with existing narrowband channel models intended for current WLAN systems at carrier frequencies of up to 5 GHz with bandwidths not exceeding 40 MHz [13], [14]. Therefore, the ultra broadband channel characterizations as presented in this paper will be necessary to develop empiric channel models required for system simulations of such upcoming THz data transmission systems [15].

The remaining paper is structured as follows. In Section II the measurement setup will be introduced in detail. Absorption coefficients of typical building materials will be given in Section III. The additional attenuation due to an object obstructing the direct ray will be examined experimentally as well as theoretically with the knife edge diffraction model [16]. Short range and indoor channel measurements based on the identified use cases are the central topics in the Sections IV-A

Manuscript received April 20, 2010; revised September 28, 2010; accepted October 26, 2010. Date of publication March 03, 2011; date of current version May 04, 2011.

S. Priebe, M. Jacob, and T. Kürner are with the Institut für Nachrichtentechnik, Technische Universität Braunschweig, Braunschweig 38106, Germany and also with the Terahertz Communications Lab, Braunschweig 38106, Germany (e-mail: priebe@ifn.ing.tu-bs.de; jacob@ifn.ing.tu-bs.de; kuerner@ifn.ing.tu-bs.de).

C. Jastrow, T. Kleine-Ostmann, and T. Schrader are with the Physikalisch-Technische Bundesanstalt Braunschweig, Braunschweig 38116, Germany and also with the Terahertz Communications Lab, Braunschweig 38106 (e-mail: christian.jastrow@ptb.de; thomas.kleine-ostmann@ptb.de; thorsten.schrader@ptb.de).

Color versions of one or more of the figures in this paper are available online at http://ieeexplore.ieee.org.

Digital Object Identifier 10.1109/TAP.2011.2122294

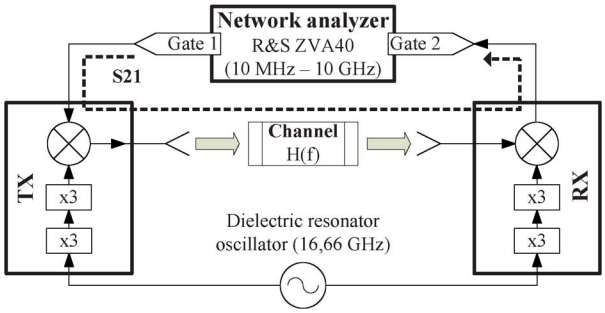

Fig. 1. The 300 GHz measurement setup.

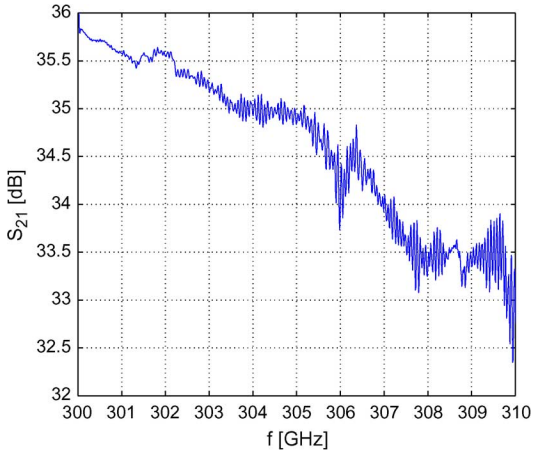

Fig. 2. Amplitude response of the 300 GHz measurement system including the antenna gain of twice 26 dBi.

and IV-C, respectively. Furthermore, the interference between the direct and a once reflected ray will be investigated including simulations according to the two-ray model [16] in Section IV-B. The measurement results are finally used as input for a first empiric path loss model before the paper is concluded in Section VI.

II. The Measurement Setup

The measurement setup consists of the core components of the 300 GHz transmission system [4] and a Rohde & Schwarz vector network analyzer (VNA) [17]. Subharmonic Schottky diode mixers are used to up-convert a baseband test signal from a Rohde & Schwarz ZVA 40 VNA to 300 GHz, which is transmitted over the channel and downconverted at the receiver. As perfect phase coherence is obligatory for correct vectorial network analysis, a common local oscillator signal generated by a dielectric resonator oscillator ($f = 16.66$ GHz) is tripled twice and then fed to the subharmonic mixers at both the TX and RX. The corresponding block diagram is shown in Fig. 1.

By recording the frequency dependent scattering parameter S_{21} [18] for the test signal frequencies f_{test} at the VNA, the channel transfer function at $f = 300$ GHz $+ f_{test}$ is measured. In the following, all S_{21} parameters specified in dB always implicitly mean the magnitude of the transfer function whereas all corresponding impulse responses are given as the relative received power over time.

Since a system error correction could only be performed at the baseband coaxial in-/output of the mixers by means of a TOSM calibration, just including the cables between VNA and the mixers, additional reference measurements allowing to correct the influence of the transmission system during postprocessing were taken with direct interconnection of the transmitter (TX) and receiver (RX) waveguides. Apart from the system losses, the depicted amplitude response (Fig. 2) also includes the antenna gains of two times 26 dBi [4] for both the TX and RX horn antenna. In the following, the antennas are always considered as a part of the transfer path so that the antenna characteristics are not discussed in more detail.

Regarding the phase response (not shown), an almost perfect linear phase was observed, corresponding to an electrical length of $l_{el,system} = 14.7$ cm. As double sideband mixers are used, the homodyne downconversion leads to an insignificant amplitude distortion between 0 dB at 300 GHz and 0.28 dB at 310 GHz due to different free-space losses in the lower and upper sideband, which needs to be corrected. The phase response is not influenced in any way. More details can be found in [17]. Multiple reflections between the transceiver modules have already been identified as a source for strong frequency selective channel transfer functions in case of direct antenna alignment [17], causing an uncorrectable error in measurement. Therefore, absorber panels have been mounted at both TX and RX for all measurements presented in this paper.

TABLE I
Measurement Parameters

Parameter	Symbol	Value
Measurement points	N	801
Intermediate frequency filter bandwidth	Δf_{IF}	10 kHz
Average noise floor	P_N	-113.97 dBm
Test signal power	P_{in}	-5 dBm
Start frequency	f_{Start}	10 MHz
Stop frequency	f_{Stop}	10 GHz
Bandwidth	B	9.99 GHz
Time domain resolution	Δt	0.1 ns
Maximum excess delay	τ_m	80 ns

In order to achieve the best possible spatial and temporal resolution of approximately 3 cm or 0.1 ns, respectively, all measurements were taken with the full available bandwidth of 9.99 GHz. The start frequency was bound to a minimum of 10 MHz by the VNA and the maximum frequency could not exceed the system limitation of 10 GHz. Due to input power restrictions of the mixers, a test signal with a power of -5 dBm was used, providing a dynamic range of approximately 85 dB for the chosen intermediate frequency filter bandwidth of $\Delta f_{IF} = 10$ kHz. The number of sweep points was chosen to 801, resulting in a maximum detectable path length of 24 m. A complete overview of all measurement parameters is given in Table I.

III. Transmission and Diffraction Measurements

Applying THz time domain spectroscopy (TDS), the TCL has already quantified the transmission losses of typical building materials [19]. Here, we determine the transparency of objects in the LOS link with the 300 GHz measurement system in transmission geometry and compare the resulting absorption coefficients with the results obtained by THz TDS. S_{21} was recorded at a module spacing of 10 cm with and without the

TABLE II
ABSORPTION COEFFICIENTS OF DIFFERENT MATERIALS

Material	$\alpha_{300\ GHz}$	$\alpha_{350\ GHz}$ [19]
Glass	9.98 cm^{-1}	9.95 cm^{-1}
MDF	4.31 cm^{-1}	4.41 cm^{-1}
Plexiglass	2.59 cm^{-1}	2.62 cm^{-1}

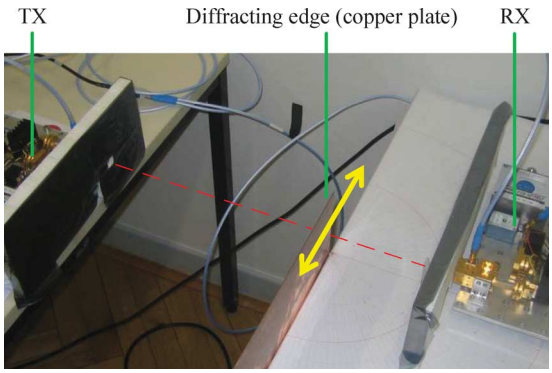

Fig. 3. Measuring the diffraction on an edge.

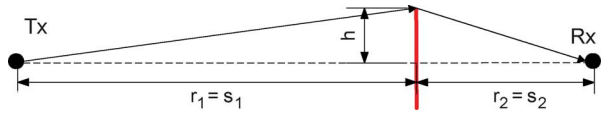

Fig. 4. Schematic drawing of the diffraction investigation setup including parameters for the knife edge model in top view.

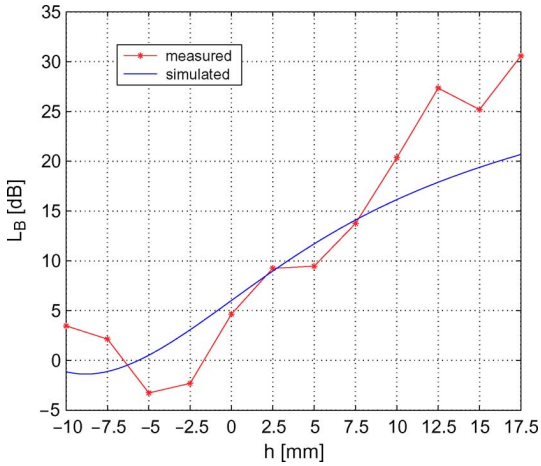

Fig. 5. Measured and simulated diffraction attenuation for different degrees of shadowing.

different samples brought into the ray path. The transmission loss was determined by subtracting $S_{21,with\ probe}|_{dB}$ from $S_{21,without\ probe}|_{dB}$. Based on the material thickness the attenuation was converted into the absorption coefficient α (Table II). Both different methods yield similar outcomes, indicating that absorption coefficients obtained in a spectrometer can be used to estimate the attenuation in an obstructed transmission path.

Assuming, e.g., a medium density fiberboard (MDF) door with a thickness of $d_{door} = 3.5$ cm or a window with $d_{window} = 2.5$ cm, absorption attenuations of approximately 65.5 and 86.7 dB are calculated. This result shows that THz WLANs will allow the reuse of the same frequency bands even in neighboring rooms without any co-channel interference to be expected. At the same time, high data security is achieved simply due to the low signal levels outside the intended service area of an access point.

Contrasting to those advantages it becomes obvious that LOS- or directed NLOS-links will be required for reliable data communication at 300 GHz. In order to systematically investigate the additional attenuation due to a gradual ray obstruction by objects, a copper plate with a thickness of 1 mm, corresponding to a sharp edge, was brought into the direct ray path at a distance of 35 cm from the TX and 15 cm from the RX (Fig. 3). This way, a worst case estimation of the obstruction attenuation, receiving only a diffracted and no transmitted ray, with given. By moving the plate orthogonally to the ray path the degree of shadowing was varied, with S_{21} being recorded in steps of 2.5 mm between $h = -10$ mm and $h = 17.5$ mm (see solid arrow in Fig. 3). The resulting diffraction attenuation L_B is calculated as the difference between $S_{21}|_{dB}$ for an obstructed and an unobstructed path as depicted in Fig. 5. The parameter $h = 0$ mm refers to the distance of the edge from the direct ray path (dashed line) with $h = 0$ mm referring to the center of the beam so that half of the first Fresnel zone [16] is shadowed. For positive values of h the direct path is blocked whereas it is increasingly unshadowed for increasingly negative h.

In the latter case, the interference of both the direct and the diffracted ray can be observed, leading to a slight gain. As expected, even small positive values of h cause a considerable additional attenuation of up to 30.7 dB, hindering ultra broadband data transmission due to seriously deteriorated signal-to-noise ratios (SNR). Therefore, fast switching from the LOS- to a directed NLOS-path becomes obligatory even for marginal ray obstructions.

In addition to the measurements, the ray obstruction by the sharp edge is simulated according to the knife edge model as described in [16] based on the geometry visualized in Fig. 4 in top view. There, the copper plate is represented by the bold red line. With $r_1 = s_1 = 35$ cm, $r_2 = s_2 = 15$ cm and $\lambda = 1$ mm, the Fresnel parameter ν is calculated as

$$\nu = h \cdot \sqrt{\frac{2}{\lambda} \cdot \left(\frac{r_1 + r_2}{r_1 \cdot r_2} \right)} = 1.381 \cdot \frac{h}{cm} \tag{1}$$

which is then used to determine the diffraction attenuation

$$\begin{aligned} L_B|_{dB} &= -20 \log \left(\left| \frac{E_{obstructed}}{E_{unobstructed}} \right| \right) \\ &= -20 \log \left(\left| \frac{1 - C(\nu) - S(\nu) + j\,(C(\nu) - S(\nu))}{2} \right| \right). \end{aligned} \tag{2}$$

$C(\nu)$ and $S(\nu)$ denote the decomposition of the Fresnel integral and are computed as described in [20, eq. (8.3a)].

A good match between simulation and measurements can be observed between $h = 0$ mm and $h = 10$ mm. For negative h, the simulation results partly overestimate the measured diffraction attenuation whereas it is underestimated beyond $h = 10$ mm. In the first case, the difference can be explained by a non-perfect placement of the copper plate in the exact distance

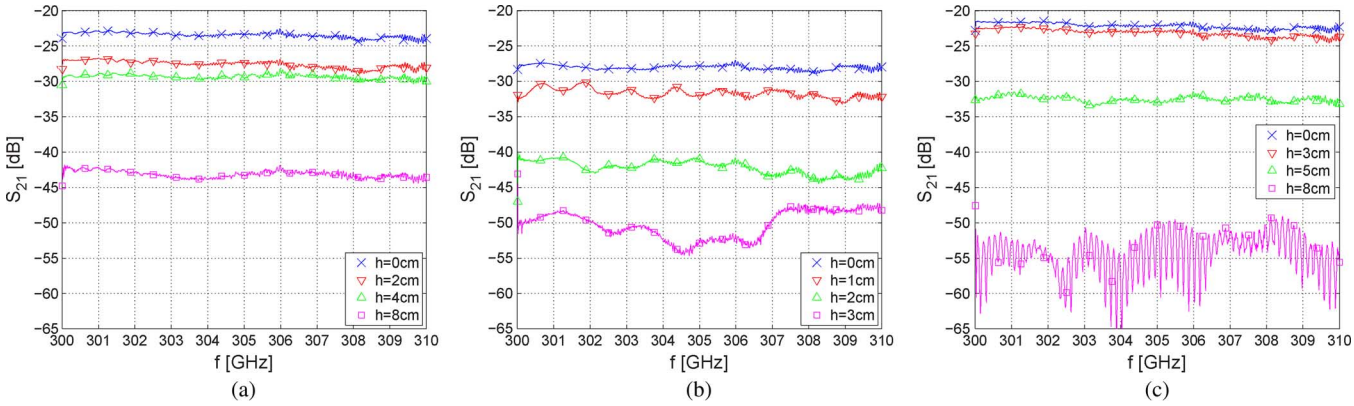

Fig. 6. Transfer functions for different module distances, misalignments and antenna types. (a) Horn antenna, $d = 40$ cm. (b) Waveguide, $d = 10$ cm. (c) Horn and PE-lense, $d = 100$ cm.

relative to the direct ray because no optical bench has been used. Moving the copper plate out of the direct path also increasingly uncovers the edge of the table on which the RX is placed, so that a second diffracted ray is received. This ray superimposes with the direct as well as with the ray diffracted at the copper plate, but has not been included in the simulation for the reason that the focus is on modeling the mere influence of the shadowing object represented by the knife edge. Moreover, the ray is received under a comparatively large incidence angle beyond the 3 dB HPBW of the horn antenna and, hence, is of minor importance. Accordingly, the measurement setup corresponds to a realistic scenario where, e.g., a person walks through the ray path, passing by the table. Here it is noteworthy that the knife edge approach has already been validated and applied for modeling the ray shadowing by moving persons between 4 and 10 GHz in [21].

From $h = 10$ mm onwards, the increasing deviation of up to 9.9 dB for $h = 17.5$ mm mainly results from the directivity of the RX horn antenna. As h increases, so does the angle of incidence of the diffracted ray at the RX. The incident diffracted ray is attenuated additionally due to the narrow main lobe for $h > 10$ mm as the modules have remained fixed and have not been pointed directly at the absorbing edge. This aspect has to be considered especially for systems with highly directional antennas by not only calculating the diffraction attenuation, but also respecting the antenna diagram of the RX antenna even for small angles of incidence. If done so, the knife edge model provides a simple and valid means for simulating the ray obstruction at 300 GHz. However, as the intention of the scenario is the investigation of the practically expected additional attenuation, the antenna influence is considered as part of the transmission path and hence has not been corrected here.

IV. Channel Characterizations

In this central chapter of the paper, we first show distance-dependent short range channel transfer functions as required for the simulation of communication systems operated on a desktop. For the reason that a perfect module positioning cannot be expected from users, each channel is investigated with regard to a certain transceiver displacement. Additionally, the influence of different antenna types is examined. Next, the frequency selectivity of ultra broadband channels caused by interference of the direct and a once reflected ray will be analyzed in detail in the second subsection. Finally, indoor channel measurements in an office environment are presented as obligatory for system simulations of future THz WLANs. Both LOS and NLOS paths will be characterized.

A. Desktop Scenario (Short Range)

Typical short range applications on a desktop can be expected to operate at distances between 20 cm and 100 cm. Suitable antenna types include open-ended waveguides, horn antennas and optional polyethylene (PE) lenses for further beam collimation. Here, the open-ended waveguides as available at the Schottky mixer outputs have been measured to provide a gain of 9.9 dBi with a 3 dB half power beamwidth (HPBW) [22] of 100°. Alternatively, 26 dBi horn antennas with 10° HPBW are used. Mounting PE lenses in front of the horn antennas enhances the gain by additional 13 dBi, each. In this case the 3 dB HPBW is reduced to 1°.

Channel transfer functions have been recorded at specific distances for each antenna type using the measurement setup shown in Fig. 7. The module spacing has been varied by moving the RX (solid arrow). By shifting the modules orthogonally to each other (dashed arrow), a certain module displacement has been simulated. The module misalignment, subsequently denoted with h, always refers to the position of best module alignment for a given distance d. In all cases the horn antenna has been mounted at the RX, whereas the TX antenna has been changed. To explicitly demonstrate the influence of the different antennas, each transfer function has been corrected by the system response, only.

For the setup with two horn antennas, a module distance of $d = 40$ cm is chosen with module displacements of $h = 0$ cm, 2 cm, 4 cm, and 8 cm [Fig. 6(a)]. Regardless of the displacement, a slight frequency-dependent channel behavior with an amplitude variation of up to 2.6 dB peak-to-peak $(h = 8$ cm$)$ can be observed. This is a consequence of nonperfect absorber panels since a ray reaches the RX after having been reflected between the RX and TX modules as described in [17]. Compared to other ultrawideband channel characterizations at 60 GHz in extreme multipath environments like a

Fig. 7. Measurement setup for short range channel characterizations.

car with amplitude variations of more than 30 dB peak-to-peak (pp) [23], the measured variation still is almost negligible.

After considering the influence of the system loss and the antenna gains, the recorded S_{21} parameter is expected to equal the free-space loss (FSL) [16]. The FSL amounts to 74 dB for $d = 40$ cm whereas a loss of approximately 75.5 dB averaged over the whole bandwidth is measured. Reasons for the deviation are the antenna mismatch at the waveguide outputs of the mixers which could not be included in the reference measurement of the system response as well as a nonperfect module alignment at $h = 0$ cm.

Even a slight antenna mispointing of $h = 2$ cm leads to additional attenuations of at least 4 dB. Whereas such a comparatively low impact on the signal-to-noise ratio (SNR) can already be taken into account in the system design by introducing a link margin, higher additional attenuations of up to 20 dB ($h = 8$ cm) can cause a serious deterioration of the achievable data rates. Apart from the different path losses, the variation of the misalignment does not influence the general channel behavior. This does not apply for the open-ended waveguide. Here, the transfer functions depicted for $d = 10$ cm with $h = 0$ cm, 1 cm, 2 cm and 3 cm show a stronger frequency dependence as the absorber panels could not be adapted to optimally fit the waveguide output [Fig. 6(b)]. Regarding the misalignment, the broad beamwidth of the RX open-ended waveguide allows comparatively high displacement lengths at short module distances while the RX horn antenna still limits the tolerable mispointing.

The PE lense is applied at $d = 100$ cm with $h = 0$ cm, 3 cm, 5 cm, and 8 cm [Fig. 6(c)]. Apart from the provided gain it serves as a spatial filter, suppressing reflections between the modules. But then, an extremely high sensitivity to displacements is induced due to the strong beam collimation. The unexpected frequency dependence that can be observed for increasing displacements is a consequence of a reflection between the RX module and the circular metal fixture of the lense, which for the reason of a flat incidence angle cannot be eliminated by the absorber panel.

In summary, two open-ended waveguides can only be operated at shortest ranges of up to several 10 cm due to the lack of a high SNR. Longer range wireless links will have to rely on highly directive antennas, accordingly. Here, a precise antenna alignment is required which is rather feasible for stationary links like the replacement of wired high speed connections or nomadic scenarios where a fixed transceiver unit has a preset area of service and only the antenna of the mobile terminal needs to be adjusted. Additional PE lenses provide the best possible SNR even over large distances but are critical regarding any displacement so that they will primarily be used for fixed radio links, e.g., for the extension of backbone networks.

B. Interference Examination Based on the Two-Ray Model

The short range channel measurements presented in the previous subsection were only taken under almost free-space conditions and did not include a reflecting plane close to the ray path. In case of placing devices on tables, near walls or nearby other reflecting objects, a strong interference of the direct and a once reflected ray can be expected despite the use of highly directive antennas. Here the focus is on a desktop scenario with two horn antennas and module distances of up to 100 cm. Apart from the measurements the scenario is simulated by applying a two-ray model [20]. Both results are compared.

To estimate the maximum possible constructive/destructive interference, the table board was simulated by a polished copper plate, having a nearly ideal reflection factor close to $r = 1$ and hence providing the maximum amplitude of the reflected path. The copper plate was placed 3.1 cm below the direct path so that the reflected ray could be received under a flat incidence angle smaller than the 3 dB HPBW of the RX horn antenna. For the measurements, typical module distances between 60 cm and 100 cm in steps of 1 mm were chosen. Fig. 8 shows the corresponding setup. Two fading dips caused by destructive interference can be found at 65.7 cm and 98.9 cm. The transfer function at $d = 65.7$ cm is demonstrated in Fig. 9, exemplarily. Here, the system loss and antenna gains are included so that the mere path loss is depicted. The multipath propagation leads to a strong frequency selectivity of the channel transfer function over the whole bandwidth, ranging from -136.7 dB to -91.4 dB. For frequencies above 306 GHz no severe fading occurs. The measured S_{21} parameter at those frequencies still exceeds the theoretical free-space loss of about 78 dB by at least 15 dB. For $f = 304.27$ GHz the highest attenuation was detected. Accordingly, this discrete frequency is chosen to demonstrate the distance dependence of the path loss around the first fading dip at 65.7 cm as shown in Fig. 10. For the simulation, $S_{21,simulated}$ is calculated as a superposition of the direct and a once reflected ray according to [20, eq. (6.22)]

$$S_{21,\text{simulated}} = 20 \cdot \log\left(\frac{\lambda}{4\pi} \cdot \left|\frac{e^{-jkd_1}}{d_1} + \frac{e^{-jkd_2}}{d_2}\right|\right) \qquad (3)$$

with $d_1 = 63.5 \cdots 67.5$ cm and $d_2 = 2 \cdot \sqrt{(0.5 \cdot d_1)^2 + h^2} = 2 \cdot \sqrt{(0.5 \cdot d_1)^2 + (3.1\ \text{cm})^2}$. Qualitatively, a good match of measurements and simulation can be observed. The slight deviation between the measured and simulated position of the fading dip can be explained by the limited spatial resolution of the measurement setup. Still, the two-ray model proves well suited for modeling the given interference situation. In case of simulating other scenarios with incidence angles beyond the 3 dB HPBW of a given antenna, the antenna diagram has to be considered, additionally.

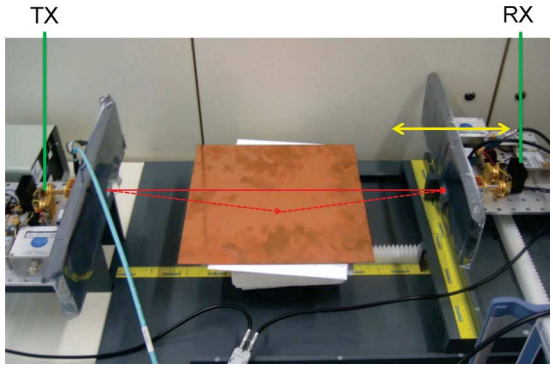

Fig. 8. Setup for interference investigations; direct ray represented by solid line, reflected ray represented by dashed line.

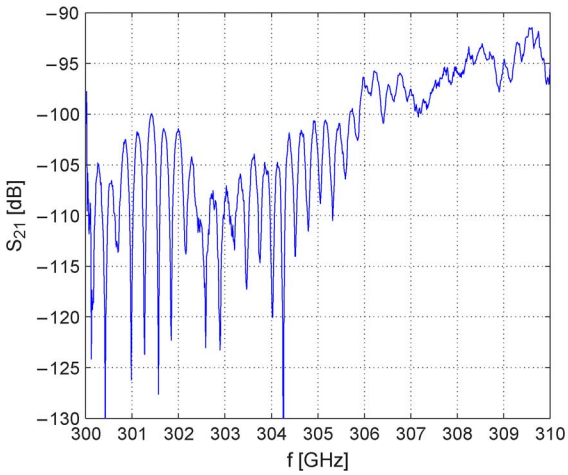

Fig. 9. Channel transfer function with copper plate ($d = 65.7$ cm).

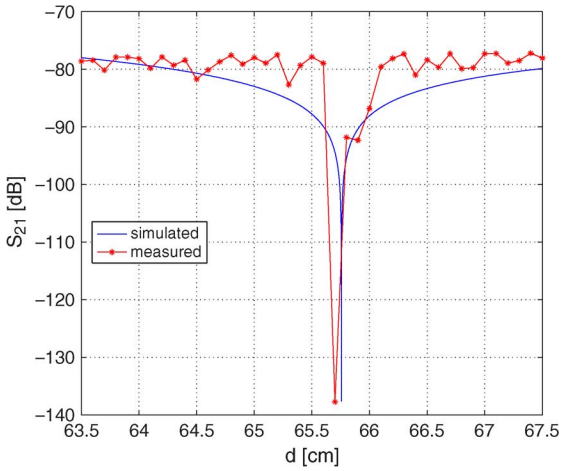

Fig. 10. Distance-dependent path loss for $f = 304.27$ GHz.

In conclusion, highly frequency selective channels may occur despite the spatial filtering by the horn antennas as soon as reflecting objects are found near the direct path, particularly within the first Fresnel zone. Regarding the prospective applications, such interference effects seriously influence the performance of ultra broadband data transmission systems and therefore will have to be considered although severe fading is expected for few discrete distances, only, as discussed in [24].

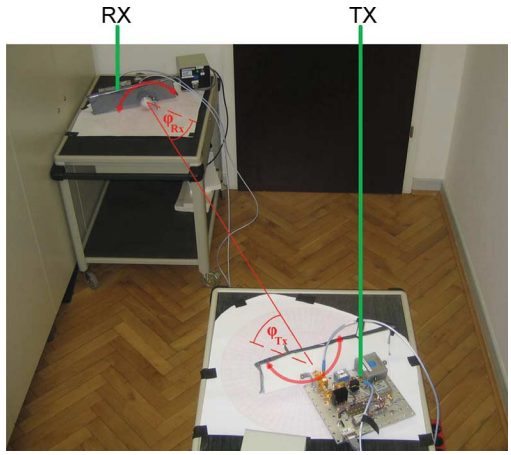

Fig. 11. The investigated office room.

C. *Office Scenario (Longer Range)*

Ray tracing at 300 GHz has already been applied by the TCL in [13] to derive a power level map and to estimate achievable data rates in a virtual indoor scenario. Still, no channel measurements required for calibration of ray tracing algorithms have been presented so far. Therefore, this sub-section focuses on the characterization of all detectable paths including once and twice reflected rays in TM polarization within a small office room with a size of $2.43\mathrm{m} \times 4.15\mathrm{m}$ limited to the horizontal plane of the TX and RX modules (Fig. 11). A schematic, full-scale illustration of all measured of all measured paths is given in Fig. 13. The room is furnished with a wardrobe and two tables on which the transceiver modules are placed. This simplified setup corresponds to a mobile device on a desktop wirelessly connected to a fixed access point in the middle of the room. Nevertheless, the presented measurements basically also apply to a situation where the access point is mounted underneath the ceiling if both modules are aligned accordingly. In this case, only the orientation of the plane of incidence, the plane of polarization and the path lengths are changed whereas the general channel behavior remains the same.

As high gain antennas with small beamwidths are required to provide a sufficient dynamic range especially for twice reflected paths, no impulse response simultaneously containing all different multipaths can be recorded. Instead, the complex channel transfer functions of the different paths are measured consecutively. If required, e.g., for the comparison of different antenna types, the complete impulse response of the scenario can then be composed of the single multipath components (MPCs). Still, highly directive antennas are most likely to be used as reasoned before so that several of the MPCs will be suppressed in any case. For the measurements, horn antennas and PE lenses are mounted at both the TX and RX. Here, the beam collimation of the lenses also helps to avoid reflections at the two table tops (cf. Section IV-B).

By turning the TX and RX, the room has been scanned for detectable paths at different combinations of angles of arrival (AoA) and angles of departure (AoD). As soon as an impulse has been found above the noise level using the time domain option of the VNA, the orientation of both modules has been

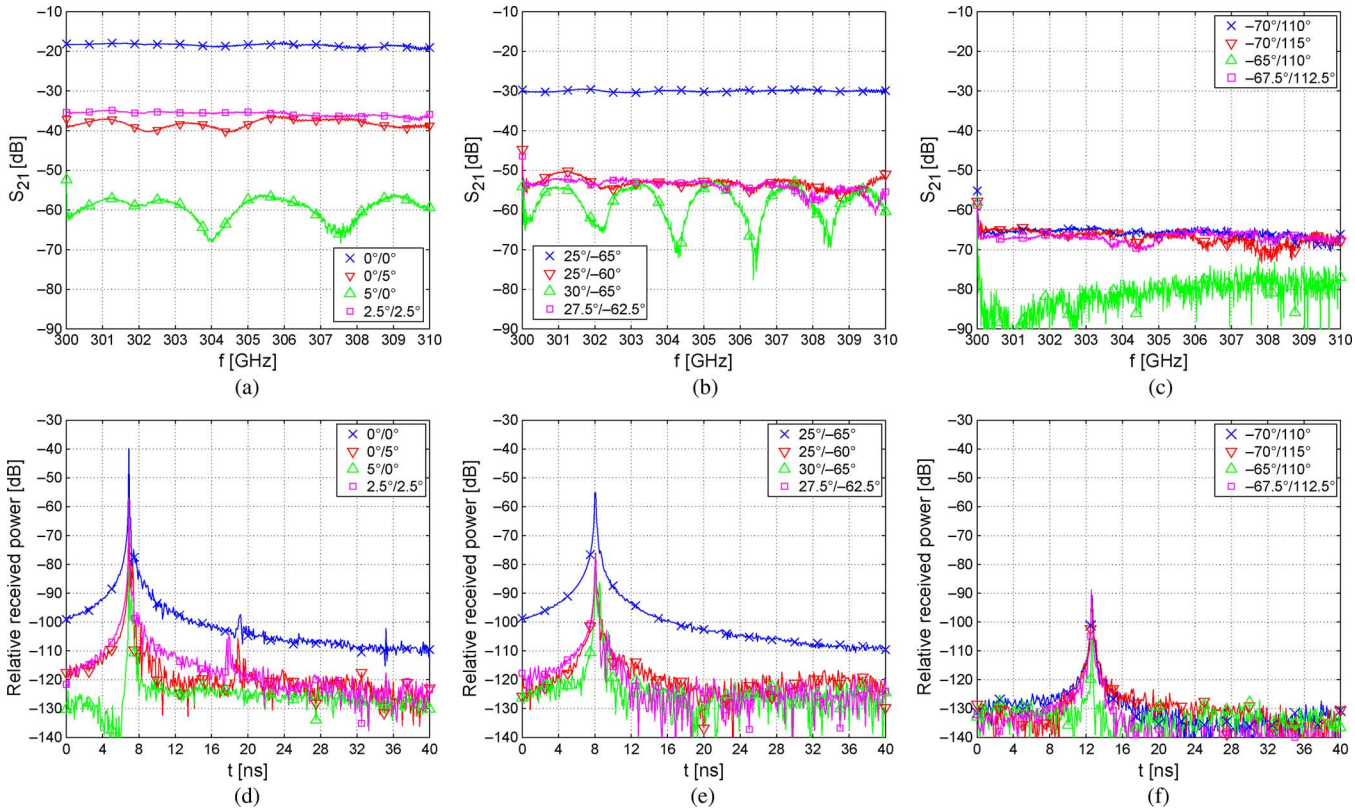

Fig. 12. Transfer functions (upper row) and relative received powers (lower row) of the direct, a once and a twice reflected path; corrected by the system loss. (a) Path (a): LOS; (b) path (c): reflection at wardrobe; (c) path (f): reflections at wall and door; (d) path (a): LOS; (e) path (c): reflection at wardrobe; (f) path (f): reflections at wall and door.

iteratively optimized in steps of $\Delta\varphi = 0.5°$ for the particular path according to the magnitude of the simultaneously displayed channel transfer function. In this setup, no reflected rays from the upper area of the room could be measured for the reason of too high path losses. The best possible module orientation for the direct path was chosen as the reference position with $\varphi_{TX} = 0°$ and $\varphi_{RX} = 0°$ (cf. straight line in Fig. 11). A positive AoA/AoD denotes mathematically positive angles φ_{TX} and φ_{RX}, respectively. Based on the best possible alignment for the respective path the module orientation of either the TX or RX is varied between $\Delta\varphi = -5°$ and $\Delta\varphi = 5°$ while the other module remains fixed. Additionally, both modules are turned by $\Delta\varphi = \pm 2.5°$ at the same time. This way, scattering processes are implicitly included in the measurements. In practice, such slight module displacements are even more likely over longer than over shorter distances as the best possible alignment becomes increasingly difficult to achieve. A complete overview of the path losses for all measured paths given by AoA and AoD is shown in Fig. 14 for the exemplary frequency of $f = 300.372$ GHz. Here, the depicted magnitude of S_{21} was corrected by the system loss and two times the antenna gain of 39 dBi. All letters refer to the labels in Fig. 13 so that the paths can be identified easily. In addition, the path characteristics are summarized in Table III for the respective best possible module alignment. Apart from the measured path loss, the theoretical free-space loss is given. The difference includes the reflection losses as well as the influence of the nonperfect module alignment and of the nonperfect positioning of the lenses in front of the horn antennas. Nevertheless, as the deviation between the FSL and the measured loss only amounts to 3.9 dB for the direct path, similar values can be assumed for the misalignment losses in the NLOS case.

TABLE III
CHARACTERISTICS OF ALL MEASURED PATHS FOR $f = 300.372$ GHz AND BEST POSSIBLE MODULE ALIGNMENT

Path	No. of refl.	Length	Measured path loss	FSL	Further losses	τ_{RMS}
(a)	0	1.67 m	90.3 dB	86.4 dB	3.9 dB	16.5 ps
(b)	2	2.93 m	129.3 dB	91.3 dB	38 dB	112.1 ps
(c)	1	2.12 m	102.4 dB	88.5 dB	13.9 dB	127.5 ps
(d)	2	4.77 m	125.3 dB	95.6 dB	29.7 dB	28.6 ps
(e)	1	2.78 m	119.6 dB	90.7 dB	28.9 dB	80 ps
(f)	2	3.45 m	145.1 dB	92.4 dB	52.7 dB	116.5 ps
(g)	1	2.8 m	120.9 dB	90.9 dB	30 dB	72.1 ps
(h)	2	3.51 m	128.4 dB	92.9 dB	35.5 dB	117.2 ps

Exemplary detailed channel transfer functions and power delay profiles of the LOS, a once and a twice reflected path are given in Fig. 12. For lack of angle-dependent antenna frequency responses, all depicted transfer functions include the inherent system losses, only. The labels of the different graphs refer to the AoA and AoD which are denoted with $\varphi_{TX}/\varphi_{RX}$, where the best possible alignment is indicated by the cross marker. Displacements of $\Delta\varphi_{TX} = 0°/\Delta\varphi_{RX} = -5°$ (downwards oriented triangle marker), $\Delta\varphi_{TX} = 5°/\Delta\varphi_{RX} = 0°$ (upwards oriented triangle marker), and $\Delta\varphi_{TX} = 2.5°/\Delta\varphi_{RX} = 2.5°$ (square marker) with regard to the respective best alignment are chosen for demonstration.

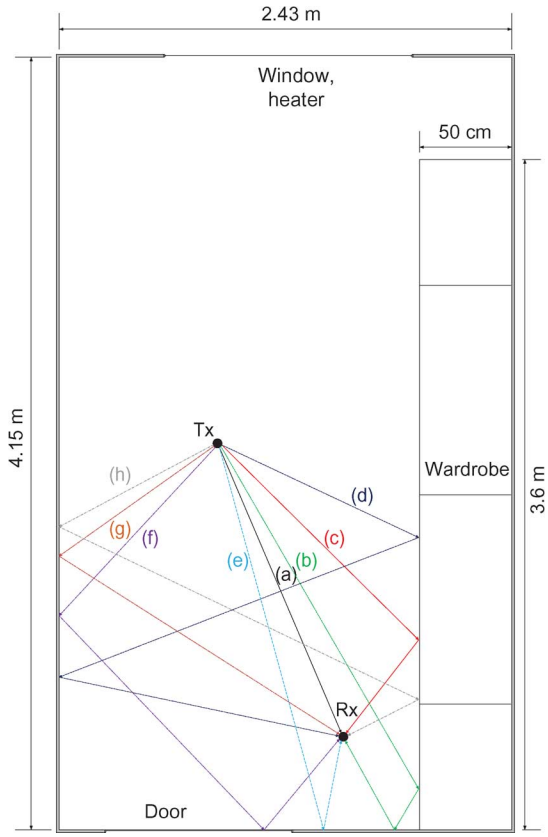

Fig. 13. All paths measured in the indoor scenario.

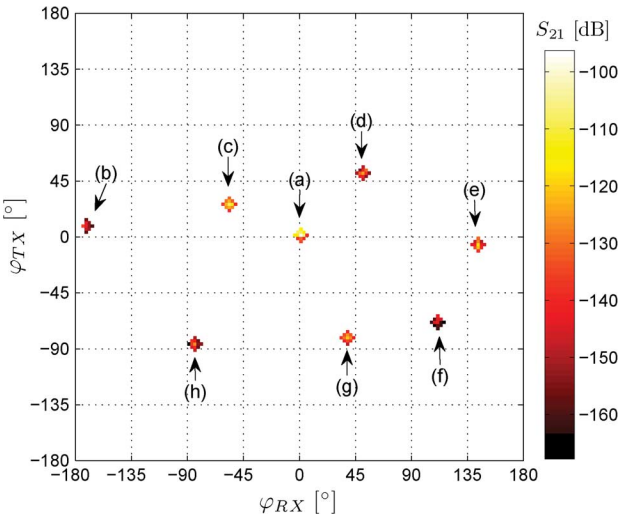

Fig. 14. Path losses of the detected paths by angle of arrival and departure for $f = 300.372$ GHz.

Almost flat transfer functions are observed over the whole bandwidth in case of no misalignment for all paths. In contrast to the short range measurements, the impulse responses do not show a multipath due to reflections between the TX and RX module apart from the LOS case. This can be explained by high reflection losses. Turning either the TX or the RX by $\Delta\varphi = 5°$ causes additional attenuations of at least 17.1 dB in the LOS case [Fig. 12(a)] and approximately 20 dB for the once reflected paths [Fig. 12(b)]. Corresponding values cannot be given for twice reflected rays as the amplitude of the transfer functions has already been too close to the noise floor [Fig. 12(c)]. Here it is noteworthy that $S_{21}|_{\varphi_{TX}=0°,\varphi_{RX}=5°}$ does not equal $S_{21}|_{\varphi_{TX}=5°,\varphi_{RX}=0°}$ [Fig. 12(a)], which is a consequence of asymmetric lense fixtures partly shadowing the incident ray.

Concerning the maximum values, the attenuation exceeds 40 dB for certain AoAs/AoDs. On the one hand, such high attenuations result from the narrow antenna beamwidth, on the other hand they are caused by high scattering losses [25] which occur for nonspecular reflections. The influence of scattering processes can in particular be seen in Fig. 12(c) for reflections at the rough plaster wall where similar transfer functions can be observed regardless of a certain mispointing.

For the temporal channel characterization, the RMS delay spread τ_{RMS} [26] has been determined from the power delay profiles (PDP) applying noise clipping with a fixed threshold of 30 dB below the detected maximum of each respective PDP. The delay spread basically increases with the number of reflections as the narrow beam is broadened by scattering processes around the point of specular reflection. Especially, this holds true for the rough surface of the plaster wall. If the criterion $K \cdot T_{symbol} > \tau_{RMS}$ [16], [27], where K denotes a constant with $0 \leq K \leq 1$, is applied to avoid high bit error rates (BER) caused by intersymbol interference, symbol rates of up to 60 and 7.8 GSymbols/s can be transmitted over the LOS and the NLOS path (c), respectively. For these upper bounds of possible symbol rates, $T_{symbol} = \tau_{RMS}$ and $K = 1$ is assumed. Here, path (c) was chosen exemplarily as it provides the least attenuation of all NLOS rays. In general, K cannot be determined analytically as the intended BER, the modulation scheme, equalizers and the specific channel impulse response have to be considered. A threshold found in literature for BPSK is $K = 0.1$ [27].

Contrastable AoA/AoD measurements at $f = 67 \ldots 110$ GHz with two 20 dBi horn antennas in a conference room scenario as presented in [28] have yielded delay spreads of up to 1.2 ns. Compared to such delay spreads, the measured channels at 300 GHz can be considered as flat. Depending on the modulation scheme and based on the considerations above, even data rates beyond 100 Gbit/s can be achieved in the LOS case regarding the temporal channel characteristics. However, it needs to be stressed that such low delay spreads rest upon the suppression of MPCs by the antennas.

In summary, ultra broadband channels at 300 GHz provide nearly flat channel transfer functions under both LOS and NLOS conditions. Directed NLOS paths can be utilized in case of direct ray blockage with the drawback of higher attenuations. Still, antenna displacements must be avoided as much as possible especially in the NLOS case. In the future, employing beamforming [29] in combination with planar antenna arrays could offer both high gains *and* easy adaptation to module displacements.

V. An Empiric Path Loss Model

The channel measurements presented previously have shown almost flat channel transfer functions (CTFs) in all cases. Even though reflected path components have been detected in the indoor environment, the pointing of the narrow beams of the TX

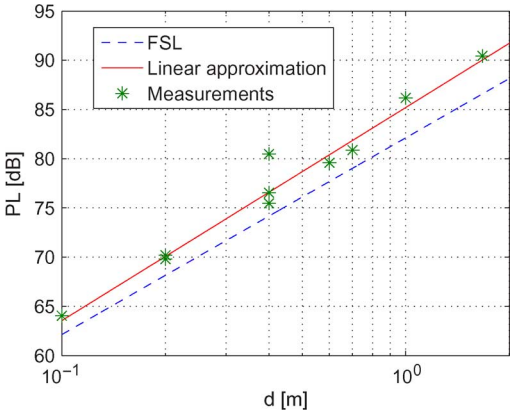

Fig. 15. Theoretical free space loss as well as measured and linearly approximated path losses averaged between 300 and 310 GHz.

and RX antennas are always optimized either for the LOS or a directed NLOS path, suppressing any other multipath component. It is noteworthy that a certain broadening of the respective received path component is observed in time domain (cf. Fig. 12), which can mainly be attributed to the computation of the inverse discrete Fourier transform of the CTF and is not caused by multipath propagation. Therefore, a simple narrowband path loss model seems reasonably sufficient as a first step towards channel modeling in the investigated scenarios. Accordingly, applying an empiric one-slope model for the path loss PL [22, eq. (4.4.1)],

$$PL = PL_0 + 10n \log\left(\frac{d}{m}\right) \tag{4}$$

is proposed. Here, d denotes the module distance in m, PL_0 refers to the path loss at $d = 1$ m and n means the propagation coefficient. Both, PL_0 and n are to be derived from experiments.

Always assuming the best possible module alignment under LOS conditions, the mere path loss is determined from the measurements for several module distances and different antennas in the first [cf. Fig. 6] as well as for the direct path [cf. Fig. 12(a)] in the second scenario. This is done by correcting the measured S_{21} parameter by the system influence and antenna gains. To account for the narrowband channel characterization, the CTFs are averaged over the whole bandwidth from 300 to 310 GHz. Then, a linear regression is applied in logarithmic domain to obtain PL_0 and n. Basically, a good agreement between the averaged theoretical free space loss, the measurements and the regression line is observed in Fig. 15. Here, PL_0 and n amount to 85.21 dB and 2.17, respectively.

Nonperfect module alignments and further unconsidered losses like antenna mismatches at the mixer outputs cause path losses exceeding the FSL by, e.g., 1.41 dB at $d = 10$ cm. Understandably, as the precise module pointing becomes increasingly difficult with larger module distances, increasing mispointing losses lead to a propagation constant slightly above 2. Furthermore, the wavelength of 1 mm can be considered small compared to the room dimensions so that no waveguiding effects are expected.

To finally evaluate the quality of the linear regression regarding the actual measurement points, the standard deviation between the measured and approximated path loss is calculated to amount to 1.44 dB. In conclusion, the simple path loss model proves well suited to describe the 300 GHz LOS channel characteristics as long as no MPCs are present. This condition can be assumed to be fulfilled, if highly directive antennas are employed. However, especially if antenna arrays with almost omnidirectional single array elements are investigated, the knowledge of the respective AoA, delay, phase, amplitude etc. of each MPC arriving at the array becomes necessary. Furthermore, multipath propagation and fading effects may also occur in rare module constellations as has been demonstrated in Section IV-B. Accordingly, the proposed model will have to be extended to a full three-dimensional broadband channel model in the near future.

VI. Conclusion

We have presented ultra broadband channel characterizations at 300 GHz using a Schottky diode mixer based measurement system. The system capabilities have been investigated. Measurements of absorption coefficients of typical building materials have been demonstrated. The diffraction at an edge has been examined and modeled as an estimate of the additional ray attenuation caused by ray blockage. It has shown, that even a slight shadowing of the direct ray will lead to high additional attenuations so that the utilization of a directed NLOS path becomes necessary. Regarding the measurement setup, the precision of the measurements compared to the simulations is limited due to the fact that no optical bench has been employed.

In addition, a short range desktop scenario and a small indoor office scenario have been considered for the channel measurements. In both cases, channel transfer functions have been presented also with regard to module misalignments. Additionally, interference investigations have been carried out according to the two-ray model. As highly directive antennas have been used, it has proven necessary to avoid even slight displacements. The analysis of the temporal path characteristics in the indoor scenario has shown that symbol rates of up to several 10 GSymbols/s can be achieved for the channel still to be considered flat. This finding basically allows for a rather simple design of THz transceivers because only rather simple or even no equalizers are required. As a concluding result, an empiric narrowband path loss model has been proposed based on the observed channel transfer functions.

All measurements obtained from the isolated propagation investigations, as well as from the channel characterizations can now be used as a guideline for the design of an appropriate 300 GHz PHY layer. For integrated system simulations, the recorded channel impulse responses can also be implemented as filters to account for realistic propagation conditions in the respective scenario.

Future work based on the outcomes presented in this paper can be, e.g., the validation of a ray tracing algorithm with the measurements or the development of a more complex and realistic 300 GHz channel model, which especially requires a further extensive measurement campaign.

REFERENCES

[1] S. Cherry, "Edholm's law of bandwidth," *IEEE Spectrum*, vol. 41, no. 7, pp. 58–60, 2004.

[2] R. Piesiewicz, T. Kleine-Ostmann, N. Krumbholz, D. Mittleman, M. Koch, J. Schoebel, and T. Kürner, "Short-range ultra-broadband terahertz communications: Concepts and perspectives," *IEEE Antennas Propag. Mag.*, vol. 49, no. 6, pp. 24–39, 2007.

[3] [Online]. Available: http://www.virginiadiodes.com/

[4] C. Jastrow, K. Münter, R. Piesiewicz, T. Kürner, M. Koch, and T. Kleine-Ostmann, "300 GHz transmission system," *Electron. Lett.*, vol. 44, pp. 213–214, 2008.

[5] C. Jastrow, S. Priebe, B. Spitschan, J. Hartmann, M. Jacob, T. Kleine-Ostmann, T. Schrader, B. Spitschan, and T. Kürner, "Wireless digital data transmission at 300 GHz," *IEE Electron. Lett.*, vol. 9, pp. 661–663, 2010.

[6] T. Nagatsuma, H. Song, Y. Fujimoto, K. Miyake, A. Hirata, K. Ajito, A. Wakatsuki, T. Furuta, N. Kukutsu, and Y. Kado, "Gigabit wireless link using 300–400 GHz bands," in *Proc. Int. Topical Meeting on Microw. Photon. (MWP)*, Oct. 2009, pp. 1–4.

[7] D. Britz, Evolution of Extreme Bandwidth Personal and Local Area Terahertz Wireless Networks *IEEE P802.15-15-10-0162-00-0thz* [Online]. Available: https://mentor.ieee.org/802.15/dcn/10/15-10-0162-00-0thz-evolution-of-extreme-bandwidth-personal-and-local-area-terahertz-wireless-networks-white-paper.pdf, 2010

[8] F. Okano, M. Kanazawa, K. Mitani, K. Hamasaki, M. Sugawara, M. Seino, A. Mochimaru, and K. Doi, "Ultrahigh-definition television system with 4000 scanning lines," in *Proc. NAB Broadcast Eng. Conf.*, 2004, pp. 437–440.

[9] T. Bird, "Terahertz radio systems: The next frontier?," presented at the Workshop on the Appl. Radio Sci., Leura, Australia, Feb. 15–17, 2006.

[10] R. Piesiewicz, M. Jacob, J. Schoebel, and T. Kürner, "Influence of hardware parameters on the performance of future indoor THz communication systems under realistic propagation conditions," in *Proc. Radar Conf. 2007 (EuRAD 2007)*, 2007, pp. 327–330.

[11] C. Jansen, R. Piesiewicz, D. Mittleman, T. Kürner, and M. Koch, "The impact of reflections from stratified building materials on the wave propagation in future indoor terahertz communication systems," *IEEE Trans. Antennas Propag.*, vol. 56, no. 5, pp. 1413–1419, 2008.

[12] T. Bird, A. Weily, and S. Hanham, "Antennas for future veryhigh throughput wireless LANs," in *Proc. IEEE Antennas Propag. Soc. Symp.*, San Diego, CA, 2008.

[13] C. Chong, C. Tan, D. Laurenson, S. McLaughlin, M. Beach, and A. Nix, "A new statistical wideband spatio-temporal channel model for 5-GHz band WLAN systems," *IEEE J. Sel. Areas Commun.*, vol. 21, 2003.

[14] *IEEE Standard for Local and Metropolitan Area Networks - Telecommunications and Information Ixchange between Systems - Local and Metropolitan Area Networks - Specific Requirements Part 11: Wireless LAN Medium Access Control (MAC)and Physical Layer (PHY) Specifications Amendment 5: Enhancements for Higher Throughput*, IEEE Std. 802.11n-2009, WG802.11 - Wireless LAN Working Group.

[15] T. Kürner, M. Jacob, R. Piesiewicz, and J. Schoebel, *An Integr. Simul. Environ. Investigat. Future THz Commun. Syst.: Extended Version*, vol. 84, no. 2–3, 2008.

[16] A. Molisch, *Wireless Communication*. New York: Wiley, 2007.

[17] S. Priebe, M. Jacob, C. Jastrow, T. Kleine-Ostmann, T. Schrader, and T. Kürner, "A measurement system for propagation measurements at 300 GHz," presented at the Progress in Electromagn. Res. Symp. (PIERS), Cambridge, U.K., 2010.

[18] D. Pozar, *Microwave Engineering*. New York: Wiley, 2007.

[19] R. Piesiewicz, C. Jansen, S. Wietzke, D. Mittleman, M. Koch, and T. Kürner, "Properties of building and plastic materials in the THz range," *Int. J. Infrared and Millimeter Waves*, vol. 28, no. 5, pp. 363–371, 2007.

[20] M. Hall, L. Barclay, and M. Hewitt, "Propagation of Radiowaves," in *Propagation of Radiowaves*. Inst. Elect. Eng.: London, U.K., 1996.

[21] J. Kunisch and J. Pamp, "Ultrawideband double vertical knife-edge model for obstruction of a ray by a person," in *Proc. IEEE Int. Conf. Ultra-Wideband (ICUWB)*, 2008, vol. 2.

[22] R. Vaughan and J. Andersen, *Channels, Propagation and Antennas for Mobile Communications*. London, U.K.: IET, 2003.

[23] M. Peter, R. Felbecker, W. Keusgen, and J. Hillebrand, "Measurement-based investigation of 60 GHz broadband transmission for wireless in-car communication," presented at the IEEE 70th Veh. Technol. Conf. (VTC2009-Fall), Anchorage, AK, Sep. 2009.

[24] M. Jacob, S. Priebe, C. Jastrow, T. Kleine-Ostmann, T. Schrader, and T. Kürner, "An overview of ongoing activities in the field of channel modeling, spectrum allocation and standardization for mm-wave and THz indoor communications," presented at the IEEE Globecom, 2009.

[25] R. Piesiewicz, C. Jansen, D. Mittleman, T. Kleine-Ostmann, M. Koch, and T. KÜrner, "Scattering analysis for the modeling of THz communication systems," *IEEE Trans. Antennas Propag.*, vol. 55, no. 11, pt. 1, pp. 3002–3009, 2007.

[26] T. Sarkar, Z. Ji, K. Kim, A. Medouri, and M. Salazar-Palma, "A survey of various propagation models for mobile communication," *IEEE Antennas Propag. Mag.*, vol. 45, no. 3, pp. 51–85, 2003.

[27] T. Rappaport, *Wireless Communications: Principles and Practice*. Upper Saddle River, NJ: Prentice-Hall PTR, 2001.

[28] M. Jacob and T. Kürner, "Radio channel characteristics for broadband WLAN/WPAN applications between 67 and 110 GHz," presented at the EuCAP, 2009.

[29] B. Van Veen and K. Buckley, "Beamforming: A versatile approach to spatial filtering," *IEEE Acoust., Speech, Signal Process. Mag.*, vol. 5, no. 2, pp. 4–24, 1988.

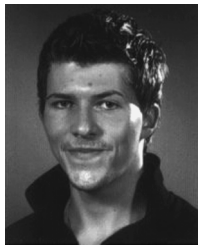

Sebastian Priebe was born in 1985. He received the Diploma degree in electrical engineering (with highest honors) from the Technische Universität (TU) Braunschweig, Germany, in 2009.

During his diploma thesis, he had already begun working on propagation mechanisms at THz frequencies, and is pursuing the Ph.D. degree in the field of future THz communication systems. He is a Research Assistant with the Institut für Nachrichtentechnik, TU Braunschweig.

Mr. Priebe was awarded a scholarship by the German National Academic Foundation.

Christian Jastrow was born in Ostercappeln, Germany, in 1981. He received the Diploma degree in electrical engineering from the Technische Universität Braunschweig, Germany, in 2008.

During his diploma thesis, he had already begun working on a 300-GHz transmission system, which was characterized and used for first data transmission by him. Currently, he is pursuing the Ph.D. degree, while working as a Research Assistant with the Electromagnetic Fields Group at Physikalisch-Technische Bundesanstalt, Braunschweig. He is primarily concerned with field exposition experiments dealing with possible nonthermal effects of THz radiation. Furthermore, he is involved in channel and propagation measurements, as well as high data rate demonstration experiments at 300 GHz.

Mr. Jastrow is a member of the VDE.

Martin Jacob (S'06) was born in Bielefeld, Germany, in 1982. He received the Diploma in electrical engineering from the Technische Universität (TU) Braunschweig, Germany, in 2007.

Currently, he is pursuing the Ph.D. degree, while working as a Research Assistant with the Institut für Nachrichtentechnik, TU Braunschweig. He is the author of more than 20 technical journal and conference papers in the field of system and channel modeling for UWB, GPS, mm-wave, and THz systems. His current research interest lies in the field of wireless communication systems at frequencies of 60 GHz and above. His work mainly focuses on channel and propagation modeling, as well as propagation measurements.

Dr. Jacob is a contributor to the IEEE 802.11ad 60-GHz WLAN channel model and is a member of the COST 2100 initiative.

Thomas Kleine-Ostmann was born in Lemgo, Germany, in 1975. He received the M.Sc. degree in electrical engineering from the Virginia Polytechnic Institute and State University, Blacksburg, in 1999, and the Dipl.-Ing. degree in radio frequency engineering and the Dr.-Ing. degree, both from the Technische Universität (TU) Braunschweig, Germany, in 2001 and 2005, respectively.

He was a Research Assistant with the Ultrafast Optics Group, Joint Institute of the National Institute of Standards and Technology and the University of Colorado, Boulder, (JILA) and with the Semiconductor Group, Physikalisch-Technische Bundesanstalt, Braunschweig, before he started working on the Ph.D. degree in the field of THz spectroscopy. Since 2006, he has been working as a permanent Scientist with the Electromagnetic Fields Group, Physikalisch-Technische Bundesanstalt. Currently, he is working on realization and transfer of the electromagnetic field strength, electromagnetic compatibility, and THz metrology. In 2007, he has become head of the Electromagnetic Fields Group.

Dr. Kleine-Ostmann is a member of the VDE and the URSI. He received the Kaiser-Friedrich Research Award in 2003 for his work on a continuous-wave THz imaging system.

Thorsten Schrader (M'97) was born in Braunschweig, Germany, in 1967. He received the Dipl.-Ing. and Dr.-Ing. degree in electrical engineering from the Technische Universität (TU) Braunschweig, in 1992 and 1997, respectively.

In 1998, he was with the EMC Test Systems LP, Austin, TX, (now ETS-Lindgren, Cedar Park, TX). In 1999, he joined the Working Group "High-frequency Measurement Techniques" of Physikalisch-Technische Bundesanstalt (PTB), Braunschweig. During 2000, he was a member of the Presidential Staff Office at PTB. In 2004, he became the Head of the Working Group "Electromagnetic Fields and Electromagnetic Compatibility." Since 2005, he has been the Head of the Department "High-frequency and Fields" and since 2006, he is also responsible for the Working Group "Antenna Measurement Techniques." His current interest is the metrology for RF quantities in the mm- and sub-mm-wave range.

Dr. Schrader is a member of VDE/VDE-GMA and VDI .

Thomas Kürner (S'91–M'94–SM'01) received the Dipl.-Ing. degree in electrical engineering and the Dr.-Ing. degree from the Universität Karlsruhe, Germany, in 1990 and 1993, respectively.

From 1990 to 1994, he was with the Institut für Höchstfrequenztechnik und Elektronik (IHE), Universität Karlsruhe, working on wave propagation modeling, radio channel characterization, and radio network planning. From 1994 to 2003, he was with the Radio Network Planning Department at the headquarters of the GSM 1800 and UMTS operator E-Plus Mobilfunk GmbH & Co KG, Düsseldorf, Germany, where he was Team Manager of Radio Network Planning and Support, where he was responsible for radio network planning tools, algorithms, processes, and parameters. Since 2003, he has been a Professor of Mobile Radio Systems at the Institut für Nachrichtentechnik (IfN), Technische Universität Braunschweig. His working areas are propagation, traffic, and mobility models for automatic planning of mobile radio networks, planning of hybrid networks, car-to-car communications, as well as indoor channel characterization for high-speed short-range systems including future terahertz communication systems. He has been engaged in several international bodies such as ITU-R SG 3, UMTS Forum Spectrum Aspects Group, and COST 231/273/259/2100.

Dr. Kürner has been a participant in the European projects IST-MOMENTUM and ICT-SOCRATES. Currently, he is chairing IEEE802.15 IG THz. He has served as Vice-Chair Propagation at the European Conference on Antennas and Propagation (EuCAP) in 2007 and 2009 and has been Associate Editor of the IEEE TRANSACTIONS ON VEHICULAR TECHNOLOGY since 2008. He is a member of VDE/ITG and VDI.